Received: 20 December 2019 | Revised: 6 February 2020 | Accepted: 26 February 2020

DOI: 10.1002/jlcr.3835

Journal of Labelled Compounds and Radiopharmaceuticals WILEY

RESEARCH ARTICLE

Arabinofuranose-derived positron-emission tomography radiotracers for detection of pathogenic microorganisms

Mausam Kalita[1] | **Matthew F.L. Parker**[1] | **Justin M. Luu**[1] | **Megan N. Stewart**[1] | **Joseph E. Blecha**[1] | **Henry F. VanBrocklin**[1] | **Michael J. Evans**[1] | **Robert R. Flavell**[1] | **Oren S. Rosenberg**[2] | **Michael A. Ohliger**[1,3] | **David M. Wilson**[1]

[1]Department of Radiology and Biomedical Imaging, University of California San Francisco, San Francisco, California

[2]Department of Medicine, University of California San Francisco, San Francisco, California

[3]Department of Radiology, Zuckerberg San Francisco General Hospital, San Francisco, California

Correspondence

: David Wilson, Department of Radiology and Biomedical Imaging, University of California, San Francisco, 505 Parnassus Ave, San Francisco, CA 94143, USA.
Email: david.m.wilson@ucsf.edu
Michael Ohliger, Department of Radiology and Biomedical Imaging, University of California, San Francisco, 1001 Potrero Ave., San Francisco, CA 94110, USA.
Email: michael.ohliger@ucsf.edu
Oren Rosenberg, Department of Medicine, University of California, San Francisco, 513 Parnassus Ave., San Francisco, CA 94143, USA.
Email: oren.rosenberg@ucsf.edu

Funding information

National Institute of Biomedical Imaging and Bioengineering, Grant/Award Number: NIH R01EB024014, NIH R01EB025985; U.S. Department of Defense, Grant/Award Number: DOD A132172; UCSF

Abstract

PURPOSE: Detection of bacteria-specific metabolism *via* positron emission tomography (PET) is an emerging strategy to image human pathogens, with dramatic implications for clinical practice. In silico and in vitro screening tools have recently been applied to this problem, with several monosaccharides including L-arabinose showing rapid accumulation in *Escherichia coli* and other organisms. Our goal for this study was to evaluate several synthetically viable arabinofuranose-derived ^{18}F analogs for their incorporation into pathogenic bacteria. *PROCEDURES:* We synthesized four radiolabeled arabinofuranose-derived sugars: 2-deoxy-2-[^{18}F]fluoro-arabinofuranoses (D-2-^{18}F-AF and L-2-^{18}F-AF) and 5-deoxy-5-[^{18}F]fluoro-arabinofuranoses (D-5-^{18}F-AF and L-5-^{18}F-AF). The arabinofuranoses were synthesized from ^{18}F$^-$ via triflated, peracetylated precursors analogous to the most common radiosynthesis of 2-deoxy-2-[^{18}F]fluoro-D-glucose ([^{18}F]FDG). These radiotracers were screened for their uptake into *E. coli* and *Staphylococcus aureus*. Subsequently, the sensitivity of D-2-^{18}F-AF and L-2-^{18}F-AF to key human pathogens was investigated in vitro. *RESULTS:* All ^{18}F radiotracer targets were synthesized in high radiochemical purity. In the screening study, D-2-^{18}F-AF and L-2-^{18}F-AF showed greater accumulation in *E. coli* than in *S. aureus*. When evaluated in a panel of pathologic microorganisms, both D-2-^{18}F-AF and L-2-^{18}F-AF demonstrated sensitivity to most gram-positive and gram-negative bacteria. *CONCLUSIONS:* Arabinofuranose-derived ^{18}F PET radiotracers can be synthesized with high radiochemical purity. Our study showed absence of bacterial accumulation for 5-substitued analogs, a finding that may have mechanistic implications for related tracers. Both D-2-^{18}F-AF and L-2-^{18}F-AF showed sensitivity to most gram-negative and gram-positive organisms. Future in vivo studies will evaluate the diagnostic accuracy of these radiotracers in animal models of infection.

KEYWORDS

arabinofuranose, imaging, infection, positron emission tomography, sugars

1 | INTRODUCTION

Bacterial infection is a major health threat in the United States and worldwide. According to the Center for Disease Control and Prevention (CDC), more than 2 million people get infected and approximately 23 000 die of bacterial infections each year in United States, with special risks posed by hospital-acquired and antibiotic-resistant microorganisms.[1] Accurate and rapid diagnosis of infection will reduce patient morbidity through effective therapeutic intervention. In addition to traditional laboratory and sampling methods, diagnostic imaging tools are frequently used in the work-up of infection and include computed tomography (CT), single photon emission CT (SPECT), magnetic resonance imaging (MRI), and hyperpolarized ^{13}C magnetic resonance (HP MR) spectroscopy. While essential, these methods frequently suffer from low diagnostic accuracy due to their inability to differentiate infection from inflammation, cancer, and rheumatologic disease and tedious data acquisition.[2–5] In light of these concerns, several groups including ours hope to develop faster, more accurate, and higher resolution positron emission tomography (PET) tools for imaging bacterial infection. Newer radiotracers derived from maltose, para-aminobenzoic acid (PABA), D-amino acids, bacterial siderophores, sorbitol, and other small-molecules have targeted bacteria-specific metabolism, with the potential for widespread clinical dissemination.[6–12] The sorbitol-derived radiotracer 2-deoxy-2-[^{18}F]fluoro-sorbitol ([^{18}F]FDS), a reduced product of [^{18}F]FDG, has been studied extensively in elegant preclinical models and more recently in patients.[13–15] This radiotracer shows high uptake in key strains of gram-negative bacteria including multidrug resistant *Escherichia coli*, *Klebsiella pneumoniae*, and *Yersinia enterocolitica.*

As shown by [^{18}F]FDS, exploiting the metabolic requirements of pathogenic bacteria for various sugar alcohols can drive the discovery of new PET tracers targeting bacterial infection. In silico and in vitro screening methods for bacteria-specific sugars, employing commercially available β-emitting ^{14}C and ^{3}H molecules, have identified numerous other candidate probes including arabinose-derived structures. Specifically, [1-^{14}C]L-arabinose showed avid and selective accumulation in *E. coli.*[16] In gram-negative bacteria, both D- and L-arabinose are converted into ribulose by the action of arabinose isomerase (Figure 1). Next, ribulokinase phosphorylates the oxygen at the 5-position generating ribulose-5-phosphate. Finally, the action of ribulose-5-phosphate-4-epimerase results in xylulose-5-phosphate, which enters the pentose phosphate pathway (PPP).[17–19] In several bacteria, additional metabolic pathways may be employed to incorporate D- and L-arabinose and their metabolites. For example, in gram-positive bacteria *Clostridium tetani*, D-arabinose-5-phosphate (A5P) isomerase catalyzes D-ribulose-5-phosphate conversion into D-arabinose-5-phosphate.[20] Beyond transport, biotransformation, and phosphorylation, there are additional mechanisms of bacteria-specific probe retention for L and D-arabinose-derived analogs. For example, the L-arabinose-binding protein (ABP) derived from the *E. coli* periplasm can bind both α- and β- anomers of L-arabinose. The ABP acts as a primary receptor for L-arabinose accumulation by bacteria.[21–24]

We hypothesized that different structural isomers of ^{18}F-labeled arabinofuranose would incorporate differentially into bacteria. In the context of high bacterial accumulation, these radiotracers could potentially be used as PET probes to distinguish acute bacterial infection from radiologic mimics. The radiotracers described in this report could also potentially be applied to imaging fungi and mammalian cells that metabolize arabinofuranoses. In this work, we developed effective radiosyntheses of four arabinofuranose-derived PET radiotracers, namely 2-deoxy-2-[^{18}F]fluoro-D-arabinofuranose (D-2-^{18}F-AF), 2-deoxy-2-[^{18}F]fluoro-L-arabinofuranose (L-2-^{18}F-AF), 5-deoxy-5-[^{18}F]fluoro-D-arabinofuranose (D-5-^{18}F-AF), and 5-deoxy-5-[^{18}F]fluoro-L-arabinofuranose (L-5-^{18}F-AF). These radiotracers were subsequently screened for bacterial incorporation in vitro.

2 | EXPERIMENTAL

2.1 | Syntheses of ^{19}F arabinofuranose standards

2.1.1 | 5-deoxy-5-fluoro-D-arabinofuranose and 5-deoxy-5-fluoro-L-arabinofuranose (D-5-F-AF and L-5-F-AF)

For detailed descriptions of syntheses for all new compounds, please refer to the Supporting Information. The compound D-5-F-AF was synthesized according to a previously published procedure.[25] The compound L-5-F-AF (**5L-5,** see B.1. in Supporting Information) was synthesized using an analogous method.

2.1.2 | 2-deoxy-2-fluoro-D-arabinofuranose and 2-deoxy-2-fluoro-L-arabinofuranose (D-2-F-AF and L-2-F-AF)

Compound D-2-F-AF was synthesized according to a previously published procedure.[26] (**2L-3**, see B.2. in Supporting Information).

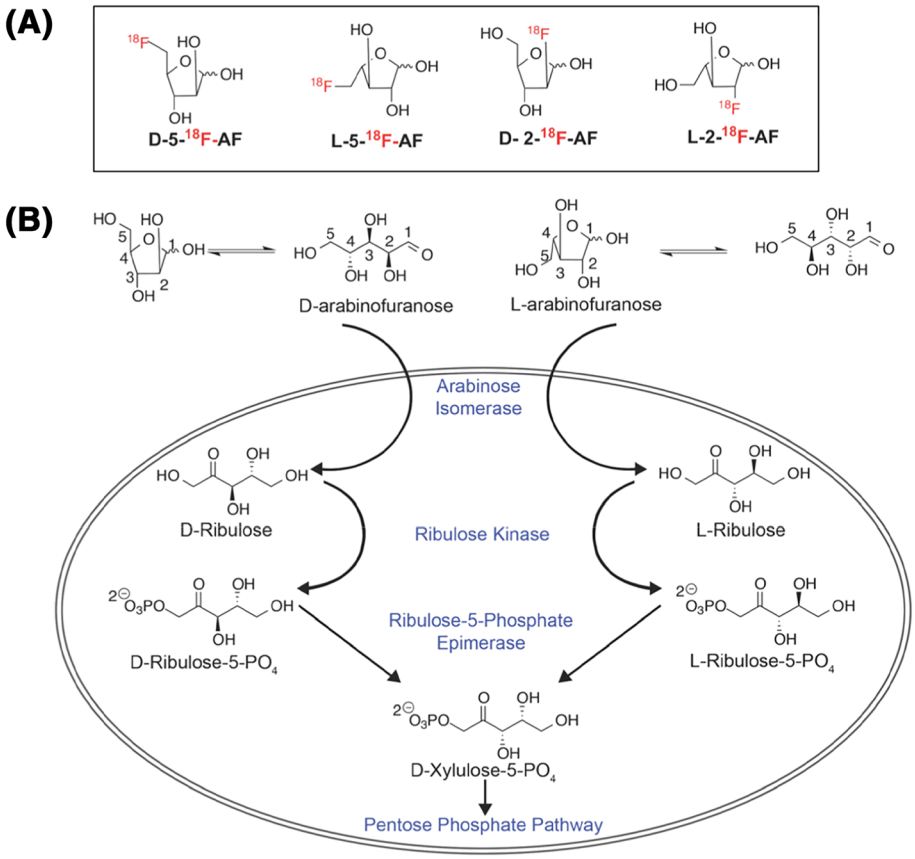

FIGURE 1 Potential mechanisms of arabinofuranose incorporation by bacteria. A, Structures of ^{18}F D- and L-arabinofuranose analogs studied and, B, metabolism of D- and L-arabinofuranose highlighting the metabolic fates of the 1-5 positions of these molecules. Arabinose isomerases (E.C. 5.3.1.3 and 5.3.1.4 for D and L forms respectively) convert D-(and L-) arabinoses into D-(and L-) ribuloses, which are subsequently phosphorylated at 5-position hydroxyl group catalyzed by ribulose kinase (E.C. 2.7.1.47 and 2.7.1.16 for D and L forms respectively). Next, ribulose-5-phosphate epimerase (E.C. 5.1.3.1 and 5.1.3.4 for D and L forms respectively) yields 2-D-xylulose-5-phosphate, which finally enters the pentose phosphate pathway. Of note, both 2- and 5-^{18}F substitution yields ^{18}F structures that are poor substrates for arabinose isomerase and ribulose kinase respectively; radiotracer incorporation for these analogs is likely mediated by transport and arabinose binding. DMSO, dimethyl sulfoxide; RT, room temperature

2.2 | Radiosyntheses of ^{18}F arabinofuranoses

2.2.1 | D-5-^{18}F-AF and L-5-^{18}F-AF

These radiotracers were synthesized in two steps (see C.2. in Supporting Information). First, the cyclotron derived ^{18}F in [^{18}O]H_2O was passed through a QMA anion exchange column eluted with 1 mL solvent (500 µL water + 500 µL acetonitrile) K_2CO_3 (2 mg) and kryptofix K222 (12 mg). This mixture was dried under nitrogen gas and vacuum with multiple additions of anhydrous acetonitrile (4X) (K_2CO_3-kryptofix K222 mix). The compound **5D-2′** or **5L-2′** (5 mg) was dissolved in anhydrous Dimethyl sulfoxide (DMSO) (500 µL) and added to the above anhydrous K_2CO_3-kryptofix K222 mix and heated to 155°C for 10 min. The R_f value of the ^{18}F-labeled compounds by radioTLC (1:1 hexanes:ethyl acetate) were comparable with the R_f values of **5L-4** and its D-counterpart standards (see Figures S1A and S2A for radioTLC), and high-performance liquid chromatography (HPLC) analysis of the ^{18}F compounds with co-injected characterized standards confirmed the identity of the esterified D- and L-5-^{18}F sugar alcohols (see Figures S1C-E and S2C-E for analytical HPLC). Second, the acetate groups were deprotected in a C-18 plus short column via 1 N NaOH. Excess ^{18}F ion was removed by passing the final compound through C-18 plus short column followed by 2× (AG11-A8-long aluminaN) columns. RadioTLC (95:5 CH_3CN:H_2O) confirmed the synthesis of D-5-^{18}F-AF and L-5-^{18}F-AF (see Figures S1B and S2B for radioTLC). The R_f value of the final products was consistent with the R_f value of the cold standard (**5L-5**).

2.2.2 | D-2-^{18}F-AF and L-2-^{18}F-AF

These syntheses were performed similarly and are fully described in section C.2. of the Supporting Information. Briefly, anhydrous ^{18}F-K_2CO_3-K222 mixture was refluxed with compound **2D-2′** (or **2L-2′**) in dry acetonitrile (500 µL). Both analytical HPLC and RadioTLC (1:1 hexane:ethyl acetate) confirmed the ^{18}F labeling (see Figures S3A and S4A for radioTLC). In both cases, the ^{18}F-labeled intermediates co-eluted with the standard D- (or L-) 2-F-OBz$_3$-α-AF (see Figures S3C-E and S4C-E for analytical HPLC). The benzoyl esters were subsequently removed on C-18 plus short column using 1 N NaOH (1 mL) for 3 min. This crude reaction mixture was neutralized with 1 N HCl and finally passed through a sequence of C-

18-AG11-A8-long aluminaN columns. The purity of the aliquots was determined in RadioTLC (95:5 CH_3CN:H_2O) (see Figures S3B and S4B for radioTLC).

2.3 | In vitro analyses of ^{18}F-arabinofuranoses

Screening studies were performed to evaluate ^{18}F arabinofuranose tracer accumulation by *E. coli* and *Staphylococcus aureus*. *E. coli* and *S. aureus* were grown aerobically in luria broth (LB) for 16 hr with agitation of 111 rpm. The cultures were pelleted at 3400 rpm for 5 minutes and resuspended in an equivalent amount of Ham's F12 media (Gibco). Following a 1/16 dilution, cultures were then incubated with 1 μCi of ^{18}F arabinofuranoses (D-2-^{18}F-AF, L-2-^{18}F-AF) at 180 rpm for 120 min. The bacterial suspensions were transferred to filter tubes (Corning Costar Spin-X) and centrifuged at 8000 rpm for 5 min. Phosphate-buffered saline was added to each tube, and the cultures were centrifuged at 8000 rpm for 5 minutes. The pellet and supernatant were separated and counted on a γ counter (Hidex Automatic Gamma Counter). Four replicates were performed for each bacterial strain.

A sensitivity study was subsequently performed to evaluate ^{18}F arabinofuranose accumulation by a panel of disease-relevant pathogens. The bacterial strains used, and their growth conditions are listed in Table S1. Bacteria strains (except *Mycobacterium marinum*) were grown aerobically in their listed media for 16 hr with agitation of 111 rpm. *M. marinum* was grown aerobically for 3 days with media replenishment every 24 hr. Culture and other experimental methods were identical to those described above. Again, four replicates were performed for each bacterial strain.

2.4 | Statistical analyses

All synthetic data including radiochemical yields and % radiochemical purities are reported as mean ± standard error. Radiochemical yields are reported with and without decay-correction for ^{18}F ($t_{1/2}$ = 110 min). in vitro data were normalized to OD_{600} for sensitivity analysis to account for differential growth rates between organisms. All statistical analysis was performed using Microsoft Excel and Prism 8.2. Four data sets were acquired for all in vitro studies (N = 4). Data were analyzed using an unpaired two-tailed Student's t-test. All graphs are depicted with error bars corresponding to the standard error of the mean.

3 | RESULTS AND DISCUSSION

3.1 | Radiosyntheses of D-2-^{18}F-AF, L-2-^{18}F-AF, D-5-^{18}F-AF, L-5-^{18}F-AF, and their corresponding ^{19}F standards

To investigate bacterial incorporation in vitro, four ^{18}F-labeled arabinofuranose sugars were elaborated. Detailed synthetic and radiosynthetic procedures, as well as compound characterization are described in the Supporting Information. The basic strategy involved synthesis of triflated, peracetylated precursors for each molecule, to mimic the most common synthetic method used for [^{18}F]FDG. For D-5-^{18}F-AF and L-5-^{18}F-AF, the increased nucleophilicity of the hydroxyl at the 5-position was used to generate orthogonally protected precursors (Figure 2A). A previous synthesis of D-2-^{18}F-AF was adapted for this purpose, while an analogous method was used for its enantiomer L-2-^{18}F-AF (Figure 2B). Diethylaminosulfur trifluoride (DAST) chemistry was then used to generate all ^{19}F standards

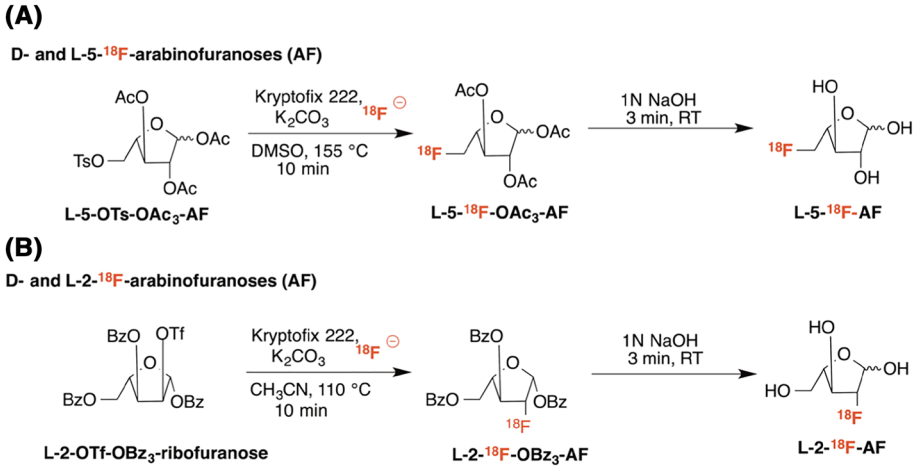

FIGURE 2 Synthesis of ^{18}F-labeled arabinofuranose-derived structures. A, D-5-^{18}F-AF and L-5-^{18}F-AF radiosyntheses B, D-2-^{18}F-AF and L-2-^{18}F-AF radiosyntheses

which were characterized fully using ^{1}H, ^{13}C, ^{19}F NMR, and high-resolution mass spectrometry. Subsequent radiosynthesis using nucleophilic ^{18}F was used to synthesize the four sugars, which were isolated via cartridge purification and characterized via radio-TLC (Figures S1A,B; S2A, B; S3A,B; and S4A,B). The summary of characterization data is as follows: D-2-^{18}F-AF (N = 12), decay-corrected yield (13.2 ± 1.6)%, end of synthesis (EOS) radiochemical yield (7.5 ± 1.2)%, and radiochemical purity (98.0 ± 2.0)%; L-2-^{18}F-AF (N = 10, decay-corrected yield (18.5 ± 2.6)%, EOS radiochemical yield (10.5 ± 1.4)%, and radiochemical purity (98.0 ± 2.0)%; D-5-^{18}F-AF (N = 3, decay-corrected yield (2.0 ± 0.2)%, EOS radiochemical yield (1.0 ± 0.1)%, and radiochemical purity (93.0 ± 1.8)%; and L-5-^{18}F-AF (N = 3, decay-corrected yield (2.2 ± 0.2)%, EOS radiochemical yield (1.1 ± 0.1)%, and radiochemical purity (94.8 ± 1.3)%.

3.2 | Screening of ^{18}F arabinofuranoses revealed accumulation of D-2-^{18}F-AF and L-2-^{18}F-AF in *E. coli*

Two of the most important bacterial pathogens are *E. coli* and *S. aureus*, which cause several clinically relevant infections. Specifically, gram-negative *E. coli* is a frequent cause of urinary tract, intestinal, and biliary infections.[27, 28] *S. aureus* is a frequent gram-positive organism cultured in skin, musculoskeletal, and bloodborne infections.[29, 30] Therefore we initially evaluated ^{18}F arabinofuranoses in these organisms prior to a broader survey of pathogens (Figure 3). Initial studies showed low accumulation of all radiotracers into *S. aureus* (mean uptake <2.0 Bq/10 million cells). Furthermore, there was lower accumulation of L-5-^{18}F-AF and D-5-^{18}F-AF in both *E. coli* and *S. aureus* (mean uptake <2.0 Bq/10 million cells). Higher incorporation was observed for L-2-^{18}F-AF and D-2-^{18}F-AF in *E. coli*; similar uptake was found for both radiotracers in *E. coli*, significantly higher than all probe combinations (P < 0.05 in all cases). The accumulation of L-2-^{18}F-AF in *E. coli* was 6-fold higher (P < 0.0001) than that in *S. aureus*, and 2.5-fold higher than that of its corresponding 5-labeled counterpart (P = 0.0001). For D-2-^{18}F-AF, accumulation in *E. coli* was 4.5-fold higher than that in *S. aureus*, and 2.4-fold higher than that of its corresponding 5-labeled counterpart (P = 0.0072). The specificity of this process for L-2-^{18}F-AF was further validated in blocking studies (Figure 4A,B). In summary, these studies indicated higher accumulation in gram-negative organisms for D-2-^{18}F-AF and L-2-^{18}F-AF and motivated further sensitivity studies.

3.3 | The sensitivities of D-2-^{18}F-AF and L-2-^{18}F-AF were evaluated in vitro using a broad panel of important human pathogens

Based on screening data, D-2-^{18}F-AF and L-2-^{18}F-AF were studied in a panel of pathogenic bacteria. These bacteria were chosen as representative gram-negative and gram-positive organisms implicated in a variety of dangerous human infections. For example, gram-negatives *K. pneumoniae* and *Pseudomonas aeruginosa* are involved in hospital-acquired disease while gram-positive *Staphylococcus epidermidis* is a cause of skin and catheter-related infections.[31, 32] A reproducible, high-throughput screening assay was developed for simultaneous evaluation of 12 living microorganisms using a single ^{18}F radiotracer synthesis. Both D-2-^{18}F-AF and L-2-^{18}F-AF were incorporated into several gram-negative and gram-positive bacteria as shown in Figure 5A,B. For D-2-^{18}F-AF the highest radioactivity was retained for *Proteus mirabilis*, *Salmonella typhimurium*, *Enterococcus faecalis and S. epidermidis* (approximately 7-8 Bq/10 million cells). The uptake levels of D-2-^{18}F-AF in these four bacteria were similar (<3-fold difference based on

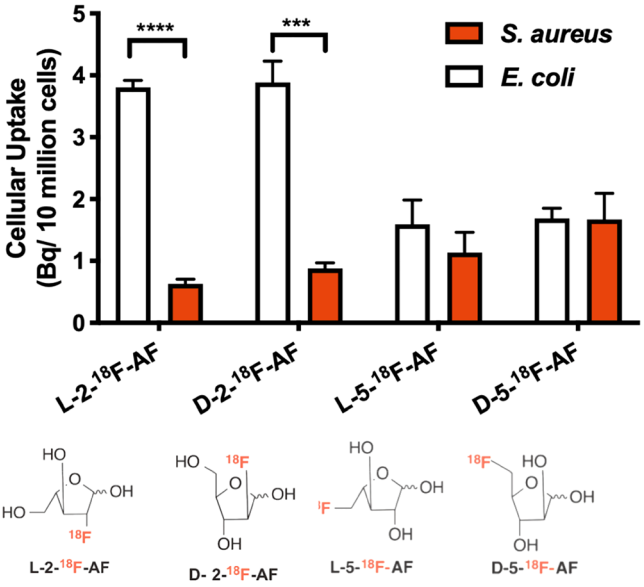

FIGURE 3 Screening of arabinofuranose-derived ^{18}F PET radiotracers in *Escherichia coli* and *Staphylococcus aureus*. in vitro uptake of L-2-^{18}F-AF in live *E. coli* was approximately 6-fold higher than that in *S. aureus* (P < 0.0001). D-2-^{18}F-AF accumulates in live *E. coli* approximately 4-fold more than in live *S. aureus* (P = 0.0002). *In vitro* uptake of D-5-^{18}F-AF and L-5-^{18}F-AF showed <1.5 Bq/10 million bacterial cells incorporation for live *E. coli* and *S. aureus* in all cases. There was no statistically significant difference in accumulation, for any combination of D- and L-5-^{18}F-AF radiotracer and organism

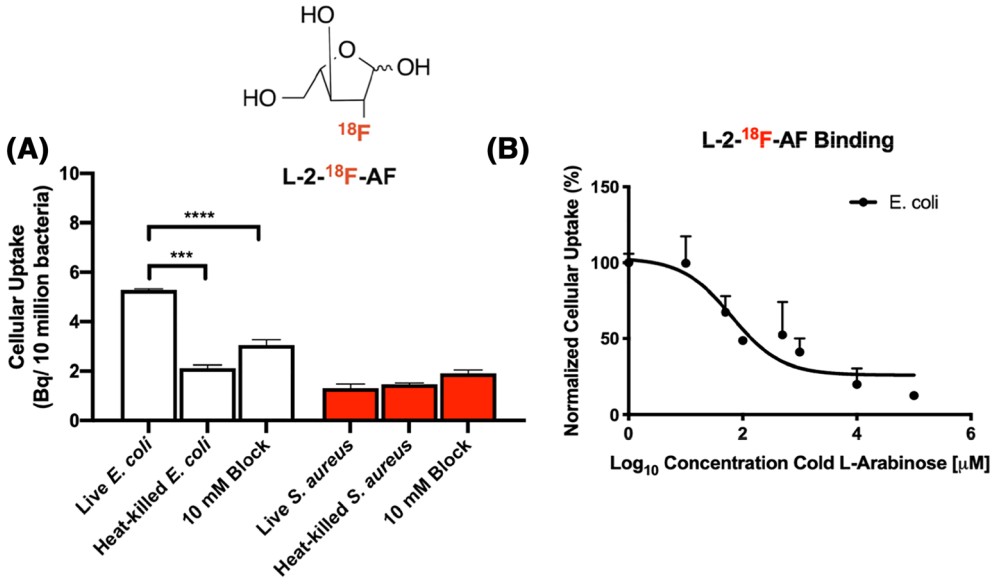

FIGURE 4 Blocking studies for L-2-^{18}F-AF. A, L-2-^{18}F-AF accumulates in live *Escherichia coli* 2.5× more than in heat-killed ($P < 0.0001$) and 1.75× more than in a blocking study using 10 mM unlabeled L-arabinose ($P = 0.0006$). This probe is retained in live *E. coli* approximately 4 times more than in live *S. aureus*. B, L-2-^{18}F-arabinofuranose uptake in *E. coli* in competition with unlabeled L-arabinofuranose at various concentrations. Cellular uptake of the radiotracer decreases as the concentration of L-arabinofuranose increases in the solution

incorporated radioactivity/10 million cells) to data recently obtained for D-[methyl-^{11}C]methionine.[33] Evaluation of L-2-^{18}F-AF showed the highest uptake in *K. pneumoniae, Acinetobacter baumannii, and M. marinum* that retained between 3.5 and 4 Bq/10 million cells. Of note, D-2-^{18}F-AF and L-2-^{18}F-AF were incorporated into both gram-negative and gram-positive species. Also significantly, there was little or no signal retained for many important pathogens for example *S. aureus*, *P. aeruginosa*, and *L. monocytogenes*.

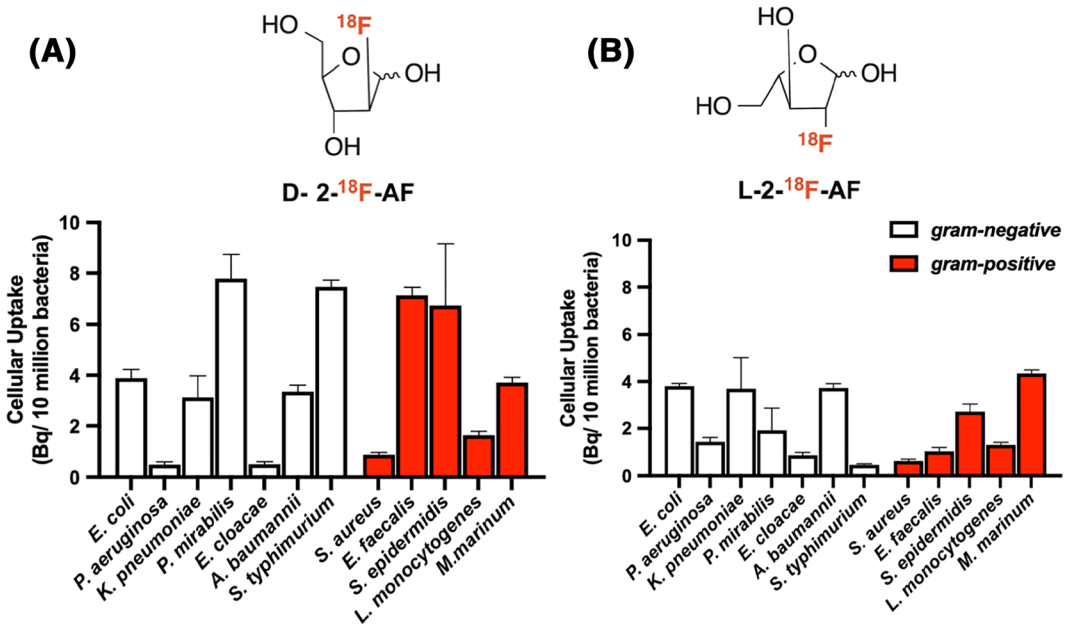

FIGURE 5 Sensitivity study in a panel of bacterial pathogens. A, D-2-^{18}F-AF showed the highest retention in *Proteus mirabilis*, *Salmonella typhimurium* and *Enterococcus faecalis*. B, L-2-^{18}F-AF showed the highest retention in several gram-positive and gram-negative bacterial strains with *Klebsiella pneumoniae*, *Acinetobacter baumannii and Mycobacterium marinum* accumulating about 4 Bq/10 million cells

4 | CONCLUSIONS

Molecular imaging methods targeting bacteria-specific metabolism have outstanding clinical potential. This potential lies in distinguishing active infection from other disease entities that appear similar on morphologic imaging (CT and MRI), allowing appropriate antimicrobial management. With the advent of multi-modality scanning, PET is particularly well suited to complement the structural information typically obtained in the work-up of infected patients. In developing PET tracers for infection, both specificity and sensitivity are important. A PET tracer specifically targeting a microbial pathway is the simplest approach; however, another strategy might be based on relative avidity of the tracer for bacterial metabolism. For this reason, we considered both D- and L-arabinofuranose-derived PET tracers.

Both D- and L-arabinofuranose-derived ^{18}F radiotracers were obtained in high radiochemical purity. Interestingly, our screening assay showed little or no bacterial incorporation of ^{18}F-arabinofuranoses with substitution at the 5-position. Although mechanistic analysis is beyond the scope of this manuscript, this finding suggests the 5-OH is necessary for retention in bacteria, perhaps based on interaction with arabinose-binding proteins. In contrast the 2-substituted molecules D-2-^{18}F-AF and L-2-^{18}F-AF demonstrated incorporation into live *E. coli*, which was not seen in heat-killed bacteria or in the presence of the nonlabeled parent sugars. The mechanisms of retention for these two tracers are currently unknown and the basis for future study. As highlighted by Figure 1, ^{18}F substitution at the 2-position would render D-2-^{18}F-AF and L-2-^{18}F-AF poor substrates for arabinose isomerase (E.C. 5.3.1.3 and 5.3.1.4 for D and L forms respectively). In this case, the bacterial retention of these probes may be mediated by their relative affinities for L-ABPs. Additional arabinofuranose-derived ^{18}F substrates that could potentially undergo biotransformation would be 3-deoxy-3-[^{18}F]fluoro-L-arabinofuranose and 3-deoxy-3-[^{18}F]fluoro-D-arabinofuranose. We made several attempts to synthesize these using an identical radiochemical strategy, without success. Several factors can impede a ring S_N2 fluorination reaction, including steric hindrance from neighboring positions, ring conformations that impede nucleophilic attack, and neighboring hydroxyl protecting groups that favor elimination.[34, 35] These 3-position arabinofuranose-derived analogs are a topic of future study.

A bacteria-targeted PET tracer would be especially valuable clinically in two scenarios, namely (a) if the tracer detects *all* or *most* pathogenic microorganisms, allowing identification of infection versus other processes, and (b) if the tracer detects important categories of organisms that are relevant to antimicrobial therapy (eg, [^{18}F]FDS that is sensitive to most *Enterobacteriaceae*). The radiotracers investigated in this manuscript D-2-^{18}F-AF and L-2-^{18}F-AF showed promising sensitivity to several microorganisms, with no apparent preference for gram-negative vs gram-positive bacteria. Furthermore, there were several important pathogens that showed low accumulation of these radiotracers most notably *S. aureus*. Future studies will investigate whether the species-specific incorporation of D-2-^{18}F-AF and L-2-^{18}F-AF can be used to noninvasively identify strains and represent an advantage in compelling clinical scenarios. Importantly, these radiotracers may also have significant application to other organisms and diseases; arabinofuranoses are metabolized avidly by fungi,[36, 37] and as highlighted by previous work, the D-arabinose isoforms in particular may find use in oncologic imaging.

ACKNOWLEDGEMENTS

Grant sponsors NIH R01EB024014, NIH R01EB025985, DOD A132172, UCSF Resource Allocation Program. The authors would also like to thank Prof Sanjay Jain and Alvaro Ordonez (Johns Hopkins University) for their assistance with in vitro methods.

CONFLICT OF INTEREST

The authors declare no competing financial interests.

AUTHOR CONTRIBUTIONS

DW, MO, and OR proposed and supervised the overall project. MK, JL, and MP obtained in vitro data. MK, MS, JB, and HVB performed the radiochemistry. MK, DW, MO, OR, RF, and ME wrote and edited the paper.

ORCID

Henry F. VanBrocklin https://orcid.org/0000-0003-2849-0841

David M. Wilson https://orcid.org/0000-0002-1095-046X

REFERENCES

1. https://www.cdc.gov/drugresistance/biggest_threats.html
2. Palestro CJ. Radionuclide imaging of osteomyelitis. *Semin Nucl Med*. 2015;45(1):32-46. https://doi.org/10.1053/j.semnuclmed.2014.07.005
3. Huang AJ, Kattapuram SV. Musculoskeletal neoplasms: biopsy and intervention. *Radiol Clin North Am*. 2011;49(1287–305):vii-1305. https://doi.org/10.1016/j.rcl.2011.07.010
4. Baker JC, Demertzis JL, Rhodes NG, Wessell DE, Rubin DA. Diabetic musculoskeletal complications and their imaging mimics. *Radiographics*. 2012;32(7):1959-1974. https://doi.org/10.1148/rg.327125054

5. Sriram R, Sun J, Villanueva-Meyer J, et al. Detection of bacteria-specific metabolism using hyperpolarized [2-13C]pyruvate. *ACS Infec Dis*. 2018;4(5):797-805.
6. Ning X, Seo W, Lee S, et al. PET imaging of bacterial infections with fluorine-18-labeled maltohexaose. *Angew Chem Int Ed Engl*. 2014;53(51):14096-14101. https://doi.org/10.1002/anie.201408533
7. Namavari M, Gowrishankar G, Srinivasan A, Gambhir SS, Haywood T, Beinat C. A novel synthesis of 6"-[18 F]-fluoromaltotriose as a PET tracer for imaging bacterial infection. *J Labelled Comp Radio*. 2018;61(5):408-414. https://doi.org/10.1002/jlcr.3601
8. Gowrishankar G, Namavari M, Jouannot EB, et al. Investigation of 6-[^{18}F]-fluoromaltose as a novel PET tracer for imaging bacterial infection. *PLoS ONE*. 2014;9(9):e107951. https://doi.org/10.1371/journal.pone.0107951
9. Zhang Z, Ordonez AA, Wang H, et al. Positron emission tomography imaging with 2-[18F]F- p-Aminobenzoic acid detects *Staphylococcus aureus* infections and monitors drug response. *ACS Infec Dis*. 2018;4(11):1635-1644. https://doi.org/10.1021/acsinfecdis.8b00182
10. Petrik M, Zhai C, Haas H, Decristoforo C. Siderophores for molecular imaging applications. *Clin Transl Imag*. 2017;5(1):15-27. https://doi.org/10.1007/s40336-016-0211-x
11. Mutch CA, Ordonez AA, Qin H, et al. [11C]Para-aminobenzoic acid: a positron emission tomography tracer targeting bacteria-specific metabolism. *ACS Infec Dis*. 2018;4(7):1067-1072.
12. Neumann KD, Villanueva-Meyer JE, Mutch CA, et al. Imaging active infection in vivo using D-amino acid derived PET radiotracers. *Scientific Reports*. 2017;7(1):7903.
13. Weinstein E, Ordonez A, DeMarco V, et al. Imaging Enterobacteriaceae infection in vivo with ^{18}F-fluorodeoxysorbitol positron emission tomography. *Sci Transl Med*. 2014;6(259):259ra-146ra. https://doi.org/10.1126/scitranslmed.3009815
14. Yao S, Xing H, Zhu W, et al. Infection imaging with (18)F-FDS and first-in-human evaluation. *Nucl Med Biol*. 2016;43(3):206-214. https://doi.org/10.1016/j.nucmedbio.2015.11.008
15. Werner RA, Ordonez AA, Sanchez-Bautista J, et al. Novel functional renal PET imaging with ^{18}F-FDS in human subjects. *Clin Nucl Med*. 2019;44(5):410-411. https://doi.org/10.1097/RLU.0000000000002494
16. Ordonez AA, Weinstein EA, Bambarger LE, et al. A systematic approach for developing bacteria-specific imaging tracers. *J Nucl Med*. 2017;58(1):144-150. https://doi.org/10.2967/jnumed.116.181792
17. Elsinghorst EA, Mortlock RP. D-arabinose metabolism in *Escherichia coli* B: induction and cotransductional mapping of the L-fucose-D-arabinose pathway enzymes. *J Bacteriol*. 1988;170:5423-5432. https://doi.org/10.1128/jb.170.12.5423-5432.1988
18. LeBlanc DJ, Mortlock RP. Metabolism of D-arabinose: a new pathway in *E. coli*. *J Bacteriol*. 1971;106(1):90-96.
19. Koirala S, Wang X, Rao CV. Reciprocal regulation of L-arabinose and D-xylose metabolism in *Escherichia coli*. *J Bacteriol*. 2016;198(3):386-393. https://doi.org/10.1128/JB.00709-15
20. Cech DL, Markin K, Woodard RW. Identification of a D-arabinose-5-phosphate isomerase in the gram-positive *Clostridium tetani*. *J Bacteriol*. 2017. https://doi.org/10.1128/JB.00246-17
21. Vyas NK, Vyas MN, Quiocho FA. Comparison of the periplasmic receptors for L-arabinose, D-glucose/D-galactose, and D-ribose. *Struct Func Simi the J Bio Chem*. 1991;266(8):5226-5237.
22. Parsons RG, Hogg RW. Crystallization and characterization of the L-arabinose-binding protein of *Escherichia coli* B-r. *J Biol Chem*. 1974;249:3602-3607.
23. Quiocho F, Ledvina P. Atomic structure and specificity of bacterial periplasmic receptors for active transport and chemotaxis: variation of common themes. *Mol Microbiol*. 1996;20(1):17-25.
24. Quiocho FA, Vyas NK. Novel stereospecificity of the L-arabinose-binding protein. *Nature*. 1984;310(5976):381-386. https://doi.org/10.1038/310381a0
25. Smellie IA, Bhakta S, Sim E, Fairbanks AJ. Synthesis of putative chain terminators of mycobacterial arabinan biosynthesis. *Org Biomol Chem*. 2007;5(14):2257-2266. https://doi.org/10.1039/b704788f
26. Clark PM, Flores G, Evdokimov NM, et al. Positron emission tomography probe demonstrates a striking concentration of ribose salvage in the liver. *Proc Natl Acad Sci U S A*. 2014;111(28):E2866-E2874. https://doi.org/10.1073/pnas.1410326111
27. Garofalo CK, Hooton TM, Martin SM, et al. Escherichia coli from urine of female patients with urinary tract infections is competent for intracellular bacterial community formation. *Infect Immun*. 2007;75(1):52-60. https://doi.org/10.1128/IAI.01123-06
28. Melzer M, Toner R, Lacey S, Bettany E, Rait G. Biliary tract infection and bacteraemia: presentation, structural abnormalities, causative organisms and clinical outcomes. *Postgrad Med J*. 2007;83(986):773-776. https://doi.org/10.1136/pgmj.2007.064683
29. McCaig LF, McDonald LC, Mandal S, Jernigan DB. Staphylococcus aureus-associated skin and soft tissue infections in ambulatory care. *Emerg Infect Dis*. 2006;12(11):1715-1723. https://doi.org/10.3201/eid1211.060190
30. Martínez-Aguilar G, Avalos-Mishaan A, Hulten K, Hammerman W, Mason EO Jr, Kaplan SL. Community-acquired, methicillin-resistant and methicillin-susceptible Staphylococcus aureus musculoskeletal infections in children. *Pediatr Infect Dis J*. 2004;23(8):701-706. https://doi.org/10.1097/01.inf.0000133044.79130.2a
31. Tumbarello M, Viale P, Viscoli C, et al. Predictors of mortality in bloodstream infections caused by Klebsiella pneumoniae carbapenemase-producing K. pneumoniae: importance of combination therapy. *Clin Infect Dis*. 2012;55(7):943-950. https://doi.org/10.1093/cid/cis588
32. Van Delden C, Iglewski BH. Cell-to-cell signaling and *Pseudomonas aeruginosa* infections. *Emerg Infect Dis*. 1998;4(4):551-560. https://doi.org/10.3201/eid0404.980405
33. Stewart MN, Parker MFL, Jivan S, et al. High enantiomeric excess in-loop synthesis of d-[methyl-^{11}C]methionine for use as a diagnostic positron emission tomography radiotracer in bacterial infection. *ACS Infect Dis*. 2020;6(1):43-49.
34. Evdokimov NM, Clark PM, Flores G, et al. Development of 2-deoxy-2-[(18)F]fluororibose for positron emission

tomography imaging liver function in vivo. *J Med Chem*. 2015; 58(14):5538-5547. https://doi.org/10.1021/acs.jmedchem.5b00569

35. Liu Z, Jenkinson SF, Vermaas T, et al. 3-Fluoroazetidinecarboxylic acids and trans,trans-3,4-difluoroproline as peptide scaffolds: inhibition of pancreatic cancer cell growth by a fluoroazetidine iminosugar. *J Org Chem*. 2015;80(9):4244-4258. https://doi.org/10.1021/acs.joc.5b00463
36. Seiboth B, Metz B. Fungal arabinan and L-arabinose metabolism. *Appl Microbiol Biotechnol*. 2011;89(6):1665-1673.
37. Li J, Xu J, Cai P, et al. Functional analysis of two L-arabinose transporters from filamentous fungi reveals promising characteristics for improved pentose utilization in *Saccharomyces cerevisiae*. *Appl Environ Microbiol*. 2015;81(12):4062-4070.

SUPPORTING INFORMATION

Additional supporting information may be found online in the Supporting Information section at the end of this article.

How to cite this article: Kalita M, Parker MFL, Luu JM, et al. Arabinofuranose-derived positron-emission tomography radiotracers for detection of pathogenic microorganisms. *J Label Compd Radiopharm*. 2020;1–9. https://doi.org/10.1002/jlcr.3835